ACS APPLIED MATERIALS & INTERFACES

Research Article

www.acsami.org

Efficiency and Air-Stability Improvement of Flexible Inverted Polymer Solar Cells Using ZnO/Poly(ethylene glycol) Hybrids as Cathode Buffer Layers

Ting Hu,[†] Fan Li,[†] Kai Yuan,[†] and Yiwang Chen*[,†,‡]

[†]Institute of Polymers/Department of Chemistry and [‡]Jiangxi Provincial Key Laboratory of New Energy Chemistry, Nanchang University, 999 Xuefu Avenue, Nanchang 330031, China

Supporting Information

ABSTRACT: The flexible inverted polymer solar cells composed of poly(3-hexylthiophene) (P3HT):(6,6)-phenyl-C61 butyric acid methyl ester ($PC_{61}BM$) blends on the flexible poly(ethylene terephthalate) (PET) substrates were fabricated, which showed improving device performance by using solution-processed ZnO/poly(ethylene glycol) (PEG) hybrids as cathode buffer layers compared to the devices using the pristine ZnO as cathode buffer layers. It is mainly attributed to the effective passivation of the ZnO surface traps, suppression of the interfacial charge recombination, decrease of the work function and improvement of the energy-level alignment between ZnO and $PC_{61}BM$. When the PEG was introduced into the ZnO, the large aggregates was dispersed and yielded large ZnO nanoclusters containing less domain boundaries. The performance of devices with ZnO/PEG6000 (with averaged molecular weight of 6000) hybrids exhibited the best power conversion efficiency (PCE) of 3.3% compared to the devices with ZnO/PEG400 (with averaged molecular weight of 400) and ZnO/PEG20000 (with averaged molecular weight of 20000). It was found that the short PEG backbone (e.g., M_w = 400) containing less oxygen could not effectively passivate ZnO surface traps, meanwhile, longer PEG backbone (e.g., M_w = 20000) could lead to the formation of the charge transport barrier because of the insulating nature of PEG. Furthermore, solar cells with the ZnO/PEG buffer also showed better air-stability. The 23% degradation was observed after 14 days, compared to the 45% degradation of devices with the pristine ZnO buffer. In addition, due to the simplicity and low-temperature process, the ZnO/PEG hybrids can be well-suitable as cathode buffer for large area roll-to-roll manufacturing of printed polymer solar cells.

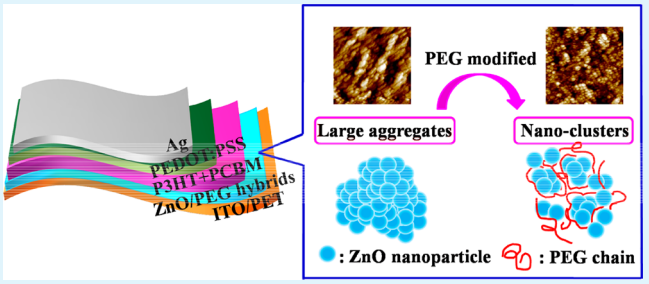

KEYWORDS: *polymer solar cells, inverted devices, hybrids, nanocomposites, surface traps, cathode buffer layers*

1. INTRODUCTION

Polymer solar cells (PSCs) based on polymer−fullerene composites have attracted extensive research because of their advantages of being renewable, low cost, and able to be fabricated by a roll-to-roll process on flexible substrates.[1−4] In the field of PSCs, bulk heterojunction (BHJ) structures based on the composites of conjugated polymers and fullerenes of interpenetrating networks are the most intensely studied. Significant efforts have been applied toward improving the competitive power conversion efficiencies (PCEs) and the long-term air stability of PSCs.[5−11]

The conventional BHJ PSCs are designed with a low work function metal cathode on top and indium tin oxide (ITO) anode coated with poly(3,4-ethylenedioxythiophene):poly-(styrenesulfonate) (PEDOT:PSS) at bottom. However, the low-work-function metal cathode is air-sensitive, and the PEDOT:PSS anode buffer layer is acidic and hygroscopic, which can degrade the performance of PSCs in conventional device configuration.[12,13] An effective pathway to solve this issue is to adopt an inverted device has been developed.[14,15] In inverted device architecture, a high work function metal is used as anode (Ag or Au), whereas an n-type metal oxide cathode buffer layer such as zinc oxide (ZnO) and titanium oxide (TiO_x) inset between the ITO cathode and active layer.[2,16] In particular, because of the high electron mobility in thin films (0.61 $cm^2\ V^{-1}\ s^{-1}$), good photophysics property and simplicity of synthesis, ZnO has been widely used as cathode buffer layers. Moreover, because of quantum confinement, the energy level and optical band gap of ZnO nanoparticle can be adjusted by the size and shape.[17−19] However, the distribution of ZnO nanoparticles is poor and adsorbed oxygen in film state as cathode buffer layer.[4] In this sense, it is necessary to develop a uniform ZnO nanoparticle film with low-defect so as to further to enhance the performance of inverted PSCs. The self-assembled monolayer treated ZnO is a potential method for reducing the defect of ZnO.[20−23] Recently, it was reported that

Received: April 9, 2013
Accepted: June 5, 2013
Published: June 5, 2013

the ZnO/polymer hybrids could effectively overcome these problems.[4,19,24,25] Among them, poly(ethylene glycol) (PEG) or poly(ethylene oxide) (PEO) with the same backbone was widely investigated. ZnO nanoparticles treated by various amounts of PEG as the cathode buffer layers have been investigated, which demonstrated that the PEG could reduce area of ZnO domain boundaries, decrease the series resistance and change the electron affinity of ZnO.[19] Meanwhile, the PEO also has been used to passivate the surface traps of ZnO nanoparticles and suppress the carriers to recombine.[24] However, in the studies mentioned above, the molecular weight of the PEG or PEO was not necessarily to consider. Meanwhile, the air-stability of the devices using ZnO/PEG hybrids or ZnO/PEO hybrids as cathode buffer layers is not assessed.

Herein, the flexible inverted PSCs based on poly(3-hexylthiophene) (P3HT):(6,6)-phenyl-C61 butyric acid methyl ester ($PC_{61}BM$) blends on the flexible poly(ethylene terephthalate) (PET) substrate were fabricated, which showed device performance and air-stability improvement by using the ZnO/PEG hybrids as cathode buffer layers. In the ZnO/PEG hybrids, PEG plays a role as a surfactant for ZnO nanoparticles, which could disperse the large aggregates and yield large ZnO nano-clusters including less domain boundaries. It is proposed that the PEG chains can effectively wrap around the ZnO nanoparticle surface and share their lone electron pair of oxygen in the backbone with ZnO nanoparticles, passivating the shallow trap sites of ZnO. Meanwhile, the PEG also could decrease the effective work function of ZnO and improve the energy-level alignment, leading to large build-in potential and improving charge mobility. As a consequence, both short circuit current density (J_{sc}) and fill factor (FF) of the inverted PSCs using ZnO/PEG hybrids as cathode buffer layers were considerably improved compared to those of devices using pristine ZnO as cathode buffer layer. The effects of PEG molecular weight on the properties of ZnO buffer layer, as well as the device efficiency and air-stability, were discussed in detail.

2. EXPERIMENTAL SECTION

Materials. The P3HT (M_w = 60 000−75 000, PDI = 1.7−1.9; Rieke Metals Inc), $PC_{61}BM$ (99.5%; Nano-C) and PEG (M_w = 400, 6000, 20000; Aldrich) was used as received. ZnO was synthesized following the process reported by Beek et al.[26] The general procedure for the preparation of ZnO as follows: 1.23 g of zinc acetate dihydrate ($Zn(CH_3COO)_2{\cdot}2H_2O$, 98%, AR, Aldrich) was dissolved in methanol (55 mL) at 60 °C under vigorous stirring. 25 mL of KOH solution (90%, AR, Aldrich, 0.34 mmol mL^{-1}) was dropped into the $Zn(CH_3COO)_2{\cdot}2H_2O$ solution in 20 minutes under vigorous stirring. The reaction was held at 60 °C for additional 2 h to yield a homogeneous, clear, and transparent solution, and then left the solution alone to precipitate for another 2 h. Precipitate was separated by centrifugation and was washed twice with methanol. We used the methanol and 1-butanol as the co-solvent in volume ratio of 1:1 to disperse the ZnO nanoparticles, with the ZnO concentration of 16 mg mL^{-1}. Herein, we named these PEG polymers in the form of PEG400, PEG6000, and PEG20000, which represents their molecular weights of 400, 6000, and 20 000, respectively. The ZnO solutions were then mixed with PEG400, PEG6000, and PEG20000 and sonicated for over half an hour. After sonication, the solution of ZnO/PEG hybrids changed to almost transparent and kept stable over 2 weeks, whereas the pristine ZnO solution remained slightly translucent and unstable.

Fabrication of Inverted Polymer Solar Cells. ITO-coated flexible PET substrates (35 Ω cm^{-2}) were cleaned with detergent, deionized water, and isopropyl alcohol and dried by nitrogen flow followed by plasma treatment for 10 min. After cleansing, a 35 nm thick ZnO or ZnO/PEG solutions were then spin coated on top of the ITO/PET substrates as cathode buffer layers, and dried in the glove box for 1 h. The blended solution was prepared by dissolving P3HT and $PC_{61}BM$ with 10 mg mL^{-1} each in 1,2-dichlorobenzene and was stirred in glovebox at 60 °C overnight, which was spin coated on top of the cathode buffer layer producing a 80 nm thick active layer and dried in the glove box for 2 h. A mixture solution of PEDOT:PSS (Baytron P AI 4083, Bayer AG) and isopropyl alcohol (1:5, v/v) was spin coated on the top of the active layer as anode buffer layer, then baked at 140 °C for 20 minutes. Finally, anode Ag (90 nm) was deposited on the top of the anode buffer layer by thermal evaporation in a high vacuum (<1 × 10^{-6} Torr). The cell area was 4 mm^2 and 12 mm^2. Current−voltage (J−V) characteristics were tested using Keithley 2400 Source Meter in the dark and under 100 mW·cm^{-2} simulated AM 1.5 G irradiation (Abet Solar Simulator Sun2000). Incident photon-to-current efficiency (IPCE) were measured under monochromatic illumination (Oriel Cornerstone 260 1/4 m monochromator equipped with Oriel 70613NS QTH lamp), and the calibration of the incident light was performed with a monocrystalline silicon diode.

Characterization. Ultraviolet−visible (UV−vis) absorption spectra were measured in PerkinElmer Lambda 750 spectrophotometer. Fluorescence measurements for photoluminescence (PL) of the ZnO samples were carried on a Hitachi F-7000 spectrofluorophotometer with a xenon lamp as the light source. The excitation wavelength was 325 nm. The crystallinity of the samples were characterized by the X-ray diffraction (XRD), using a Bruker D8 Focus X-ray diffractometer operating at 30 kV and 20 mA with a copper target (λ = 1.54 Å) under a scanning rate of 1°/min. Transmission electron microscopy (TEM; JEOL, JEM-2100F, field-emission transmission electron microscope) investigations were tested on holey carbon-coated copper grids. The morphologies of the ZnO nanoparticles and ZnO/PEG hybrids were characterized by an atomic force microscope (AFM) (Digital Instrument Nanoscope 31). Ultraviolet photo-electron spectroscopy (UPS) measurement was carried on AXIS-ULTRA DLD spectrometer (Kratos Analytical Ltd.) using He (I) (21.2 eV) as monochromatic light source. The thicknesses of all the layers were measured by surface profilometry (Alpha-Step-IQ). Water contact angle measurements for all samples were characterized on JC2000A contact angle instrument.

3. RESULTS AND DISCUSSION

In the experiment, the ZnO/PEG hybrids were empolyed as the cathode buffer layers in inverted P3HT:$PC_{61}BM$ PSCs on flexible PET substrates. Figure 1a showed the inverted device

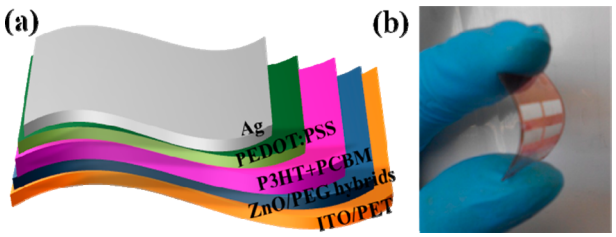

Figure 1. (a) Device structure used in this work and (b) picture of the flexible device.

architecture employed in this work. The detailed fabrication process is described in the Experimental Section. A picture of the flexible device is given in Figure 1b. Here, we emphasiz the influence of PEG molecular weight on the the properties of ZnO cathode buffer layers and the performance of PSCs.

The illuminated current−voltage (J−V) curves of flexible inverted P3HT:$PC_{61}BM$ solar cells using ZnO hybridized with PEG of various molecular weights as cathode buffer layers were shown in Figure 2a. The devices using pristine ZnO as cathode buffer layer were also fabricated for comparison. Figure 2b

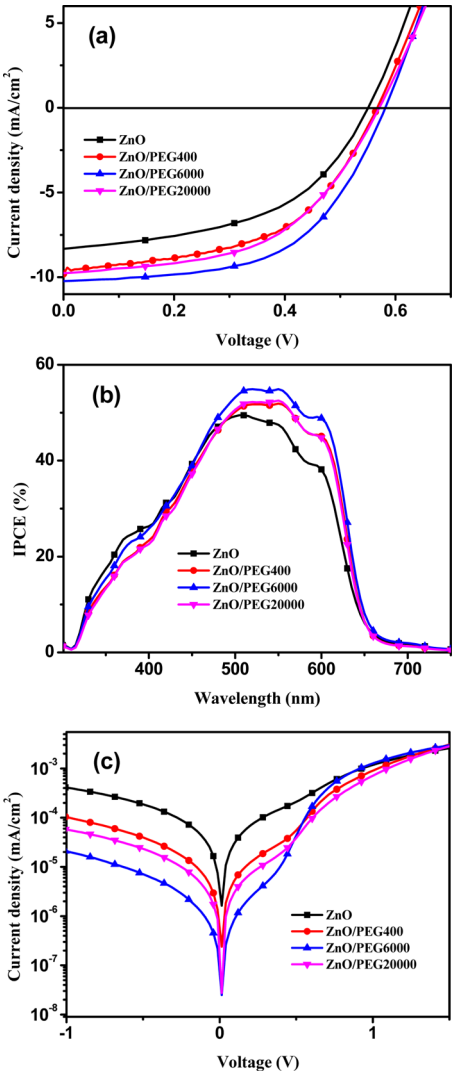

Figure 2. (a) Illuminated $J-V$ characteristics, (b) IPCE spectra and (c) dark current of devices based on P3HT:$PC_{61}BM$ blends using ZnO, ZnO/PEG400, ZnO/PEG6000, and ZnO/PEG20000 as cathode buffer layers.

shows IPCE spectra of the devices and the results confirm the tendency of J_{sc} upon applying the ZnO/PEG hybrids as the cathode buffer layers. Table 1 summarized the corresponding device parameters. As shown in Table 1, the device using pristine ZnO as cathode buffer layer showed an open circuit voltage (V_{oc}) of 0.55 V, a J_{sc} of 8.36 mA cm^{-2}, a FF of 49.7% and a PCE of 2.3%. The device performance was improved when ZnO hybridized with PEG of various molecular weights was used as cathode buffer layer. From the $J-V$ curves, it was found that the best performing PSC was based on the ZnO/PEG6000 hybrids cathode buffer layer which exhibited 3.3% PCE with V_{oc} = 0.58 V, J_{sc} = 10.19 mA cm^{-2}, and a FF = 55.9%. This was attributed to its reduction of series resistance (R_s) of 10.8 Ω cm^2 in comparison to 18 Ω cm^2 of the PSCs with ZnO cathode buffer layer and elevated shunt resistance (R_{sh}). Consequently, the decreased R_s and increased R_{sh} contribute to the device performance by improving the FF and J_{sc}.[15] Figure 2c shows the $J-V$ characteristics of inverted PSCs using ZnO and ZnO/PEG hybrids as cathode buffer layers measured without illumination. It was found that the leakage current of the device with ZnO/PEG cathode buffer layer is considerably restrained, indicating that the recombination of carriers was suppressed by ZnO/PEG hybrids cathode buffer layer.[27,28] Thus, higher photocurrent of the devices using ZnO/PEG hybrids as cathode buffer layers is expected.

Figure 3 showed the variations in J_{sc}, V_{oc}, FF, and PCE, respectively. As presented in Figure 3, it could be observed that

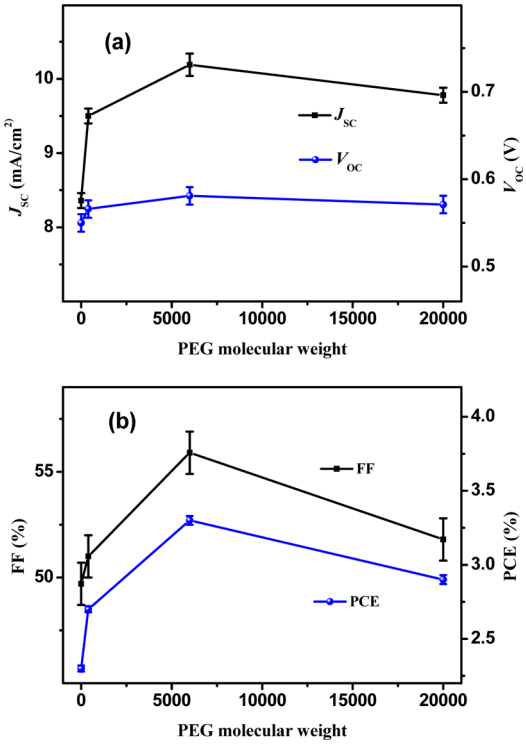

Figure 3. Effect of ZnO and ZnO/PEG with different molecular weights on photovoltaic performance such as (a) short-circuit current density and open-circuit voltage, and (b) fill factor and power conversion efficiency.

Table 1. Performance Parameters of the Devices Based on P3HT:$PC_{61}BM$ Blends Using ZnO, ZnO/PEG400, ZnO/PEG6000 and ZnO/PEG20000 as Cathode Buffer Layers

Devices	J_{sc} (mA cm^{-2})	V_{oc} (V)	FF (%)	R_s (Ω cm^2)	R_{sh} (Ω cm^2)	PCE (%)
ZnO	8.36	0.550	49.7	18	263.8	2.3
ZnO/PEG400	9.50	0.566	51.0	13.9	346.3	2.7
ZnO/PEG6000	10.19	0.581	55.9	10.8	671.1	3.3
ZnO/PEG20000	9.78	0.571	51.8	12.2	477.6	2.9

V_{oc} did not show any significant changes for all devices. Generally, the V_{oc} value not only depends on the energy difference between the highest occupied molecular orbital (HOMO) level of the donor and the lowest unoccupied molecular orbital (LUMO) level of the acceptor materials, but also depends on electrode work functions.[29] Therefore, the V_{oc} of all the devices did not significantly change because the same electron donor, electron acceptor, and ITO, Ag electrode were employed. In contrast, J_{sc}, FF, and PCE revealed variations and exhibited the same variation trend, and the highest value was observed for the devices using ZnO/PEG6000 buffer layer. It is known that the transmittance of the buffer layer makes a large

dx.doi.org/10.1021/am4013038 | ACS Appl. Mater. Interfaces 2013, 5, 5763−5770

difference in the device performance of inverted PSCs.[30] Figure S1 in the Supporting Information shows the optical transmittance spectra of ZnO and ZnO/PEG buffer layers in the UV−visible wavelength range (200−1200 nm). With all the ZnO and ZnO/PEG hybrids layers showing similar transmittance, we can infer that the optical improvement is not the main factor of the enhancement of J_{sc}. Meanwhile, XRD results showed that the addition of PEG had no obvious influence on the crystallinity of the ZnO (see Figure S2 in the Supporting Information), which also did not account for the improvement of J_{sc}.

The tuning of concentration of PEG in ZnO/PEG hybrids was thoroughly investigated as a function of the effect of hybridization on the device performance. Figure 4 and Table 2

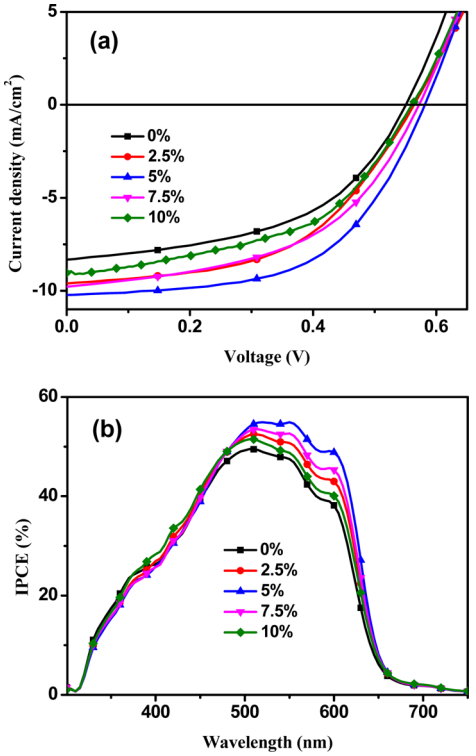

Figure 4. (a) Illuminated $J-V$ characteristics and (b) IPCE spectra of devices based on P3HT:$PC_{61}BM$ blends using ZnO hybridized with PEG6000 of different weight concentrations as cathode buffer layers.

Table 2. Performance Parameters of the Devices Based on P3HT:$PC_{61}BM$ Blends Using ZnO Hybridized with PEG6000 of Different Weight Concentrations as Cathode Buffer Layers

devices	J_{sc} (mA cm^{-2})	V_{oc} (V)	FF (%)	R_s (Ω cm^2)	R_{sh} (Ω cm^2)	PCE (%)
ZnO	8.36	0.550	49.7	18	263.8	2.3
ZnO/2.5% PEG6000	9.53	0.563	50.9	15.3	316.3	2.7
ZnO/5.0% PEG6000	10.19	0.581	55.9	10.8	671.1	3.3
ZnO/7.5% PEG6000	9.51	0.562	52.1	13.1	413.9	2.8
ZnO/10% PEG6000	9.09	0.560	50.2	17.3	294.5	2.6

showed the photovoltaic performance of PSCs with different concentrations of PEG6000 in ZnO/PEG hybrids as cathode buffer layers. In Figure 4a, as PEG6000 contents increased, the device performance was dramatically changed. The J_{sc} and FF were significantly enhanced to 10.19 mA cm^{-2} and 55.9% with a PCE of 3.3% at 5 wt % of PEG6000. The J_{sc} increased upon concentration of PEG6000 in ZnO/PEG6000 hybrids, in accordance with the change in the IPCE spectra showed in Figure 4b. Devices showed with the highest values between 500 nm and 610 nm at 5 wt % of PEG6000. The increased of IPCE spectral response was due to the enhanced light absorption and charge collection.

To evaluate the performance of the device more reasonable and reliable, we provide the device data with a larger area at 12 mm^2. Figure 5 showed the current density versus voltage ($J-V$)

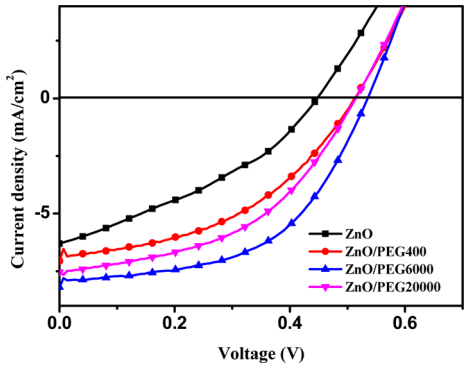

Figure 5. Illuminated $J-V$ characteristics of devices based on P3HT:$PC_{61}BM$ blends with an active area of 12 mm^2 using ZnO, ZnO/PEG400, ZnO/PEG6000, and ZnO/PEG20000 as cathode buffer layers.

Table 3. Performance Parameters of the Devices Based on P3HT:$PC_{61}BM$ Blends with an Active Area of 12 mm^2 Using ZnO, ZnO/PEG400, ZnO/PEG6000, and ZnO/PEG20000 as Cathode Buffer Layers

devices (12 mm^2)	J_{sc} (mA cm^{-2})	V_{oc} (V)	FF (%)	R_s (Ω cm^2)	R_{sh} (Ω cm^2)	PCE (%)
ZnO	6.27	0.447	35.1	37.6	216.8	1.0
ZnO/ PEG400	7.06	0.511	43.4	24.8	321.4	1.6
ZnO/ PEG6000	8.19	0.534	51.4	19.7	375.1	2.2
ZnO/ PEG20000	7.53	0.513	46.7	21.4	342.6	1.8

characteristics. Table 3 provided details of the device characteristics. Although the J_{sc} and FF of the larger area devices reduced and the efficiency of device based on ZnO/PEG6000 hybrids as cathode buffer layer remained 67% of the 4 mm^2, the efficiency of device based on ZnO buffer layer was only 43% of the 4 mm^2. This result indicated that the device using ZnO/PEG6000 hybrids as cathode buffer layer was also superior to that using pristine ZnO at large scale. The reduced power loss in an organic solar cell at large scale was attributed to the decreased sheet resistance of the cathode buffer layer.[31](Table 3)

To investigate the effect of PEG modification on surface defects of ZnO nanoparticle, we have studied the PL of ZnO modified with PEG of various molecular weights under photoexcitation at 325 nm (Figure 6). The narrow emission

dx.doi.org/10.1021/am4013038 | ACS Appl. Mater. Interfaces 2013, 5, 5763−5770

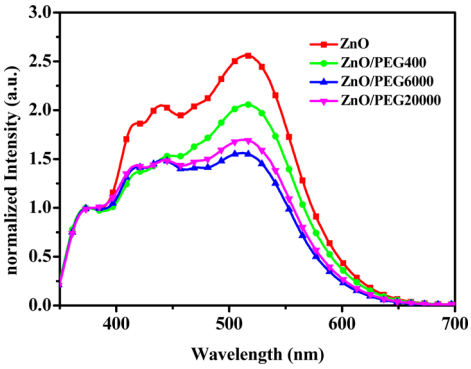

Figure 6. Normalized photoluminescence spectra of ZnO, ZnO/PEG400, ZnO/PEG6000, and ZnO/PEG20000 films.

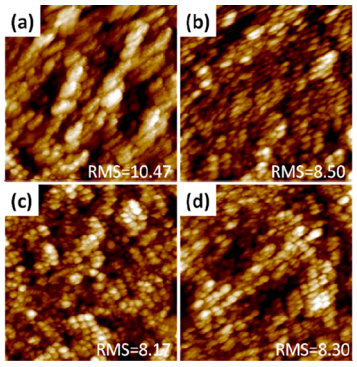

Figure 7. AFM height images (1μm × 1μm) of (a) ZnO, (b) ZnO/PEG400, (c) ZnO/PEG6000, and (d) ZnO/PEG20000 films.

band at 368 nm (3.37 eV) is assigned to exiciton emission. Meanwhile, the spectrum exhibits two wide emission bands in blue and green regions. There are two shoulders that are obvious at 420 nm (2.95 eV) and 440 nm (2.82 eV) in the blue emission originating from transitions involving Zn interstitial defect states.[32] In addition, it also can be observed that there exists the intense broad emission around 515 nm (2.41 eV) in the green emission. Various hypotheses have been proposed for green emissions, such as transition between singly ionized oxygen vacancies (V_o) and photoexcited holes, transition between electrons close to the conductive band and deeply trapped holes at V_o^{++}, surface defects, etc.[32−35] As shown in Figure 6, obviously, the defect emission of the pristine ZnO is stronger than that of the ZnO/PEG hybrids, indicating that the PEG could reduce surface traps of ZnO. It is proposed that the PEG chains can effectively wrap around the ZnO nanoparticle surface and share their lone electron pair of oxygen in the backbone with ZnO nanoparticles, which passivated the shallow trap sites of ZnO.[24,36] The reduction of ZnO traps can lower the possibility of trap-assisted recombination in the interface. It also was noted that defect emissions of ZnO/PEG6000 and ZnO/PEG20000 are weaker than that of ZnO/PEG400. We infer that the amount of lone electron pair of oxygen in the short PEG backbone (M_w = 400) is not enough to effectively coordinate with ZnO. In addition, water contact angle tests were performed for the pritine ZnO and ZnO/PEG hybrids. As shown in Figure S3, the water contact angle decreases from 46° for the ZnO film to 32° for the ZnO/PEG20000 film due to the hydrophilic property of the PEG. Figure S4 in the Supporting Information showed the water contact angle tests of ZnO and ZnO/PEG hybrids with different concentration of PEG6000. As expected, the water contact angle decreases with the increase in the concentration of PEG6000.

To investigate the morphology of ZnO and ZnO/PEG films affected by the PEG, the AFM images obtained from these ZnO and ZnO/PEG films are shown in Figure 7. As shown in Figure 7, the ZnO/PEG6000 film shows a smooth surface with root-mean-square (RMS) roughness value of 8.17 nm, while the pristine ZnO film presents a RMS value of 10.47 nm. With the performance of PSCs using different ZnO cathode buffer layers in accordance with the surface roughness, it indicates that the rougher ZnO films have more interface traps. The increase of interface traps can facilitate the possibility of trap-assisted recombination of electron, leading to the low FF of the solar cells. Hence, the reduced roughness of ZnO cathode buffer layers can be counted as a contributor to the enhanced FF. The effect of PEG modification leads to large ZnO nanocluster domains with fewer boundaries, which enhanced electron transport and decreased carrier trapping in the trap sites at boundaries.[18,37−41] As shown in the AFM images, the pristine ZnO form large aggregates. When the PEG was introduced into the ZnO, the large aggregates was dispersed and yielded large ZnO nanoclusters containing less domain boundaries. The domain boundaries of semiconductor nanocrystal clusters can catch the charge carriers with the role of energetically deep-lying trap sites.[19] Therefore, it is one of possible reasons for the improved J_{sc} of the ZnO/PEG. We suspected that the short PEG backbone (e.g., M_w = 400) is not long enough to wrap around the ZnO nanoparticle surface to form uniform nanoclusters of suitable size, but the appropriate length of PEG backbone (e.g., M_w = 6000) produced a better result with more uniform clusters and smaller domains. As to the longer PEG backbone (e.g., M_w = 20000), the insulating property should be taken into account. It can be supposed that the crimp and long insulating backbone of PEG fills up the interspace yielded the barrier of the charge transport.

To gain further insight into the variation of the morphologies of ZnO hybrided with different PEG, we also employed TEM. TEM images obtained from these ZnO films are shown in Figure 8, the pristine ZnO nanoparticles are aggregated together forming large aggregates. On the contrary, the addition of PEG stabilized the dispersion of large ZnO cluster domains with fewer boundaries, which is consistent with the results of AFM analysis.

To investigate the effect of electronic properties of ZnO and ZnO/PEG interfacial layers on the photovoltaic performance, we carried out UPS measurement to study the energy levels of pristine ZnO and ZnO/PEG hybrids cathode buffer layer. As shown in Figure 9, the high binding energy cutoff from a spectrum is E_{cutoff} (left panel, Figure 9a), which was estimated by linear extrapolation to zero at the yield of secondary electrons.[42,43] The right panel of Figure 9a shows the HOMO region. The E_{HOMO} is the onset relative to the Fermi level (E_F) of Au (at 0 eV), where the E_F was determined from the Au substrate. The HOMO energies (Figure 9b) are determined according to the following equation[43]

$$E_{HOMO} = h\upsilon - (E_{onset}^{HOMO} - E_{cutoff})$$

where $h\nu$ is the incident photon energy ($h\nu$ = 21.2 eV) for He I. Consequently, the HOMO energies for ZnO, ZnO/PEG400, ZnO/PEG6000 and ZnO/PEG20000 film are −7.57, −7.54, −7.45, and −7.49 eV, respectively. On the basis of these HOMO energies and the optical band gap (E_g = 3.38 eV) extracted from the UV−vis absorption spectra (Figure 10), the

dx.doi.org/10.1021/am4013038 | ACS Appl. Mater. Interfaces 2013, 5, 5763−5770

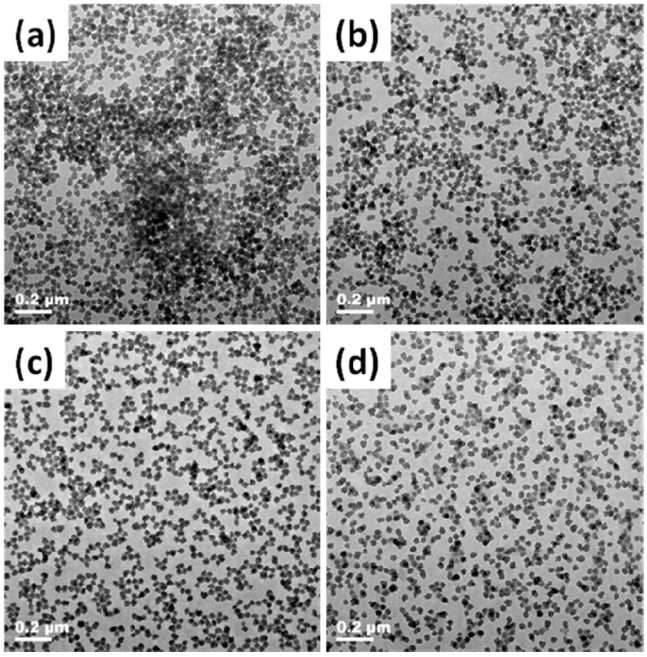

Figure 8. TEM images of (a) ZnO, (b) ZnO/PEG400, (c) ZnO/PEG6000, and (d) ZnO/PEG20000.

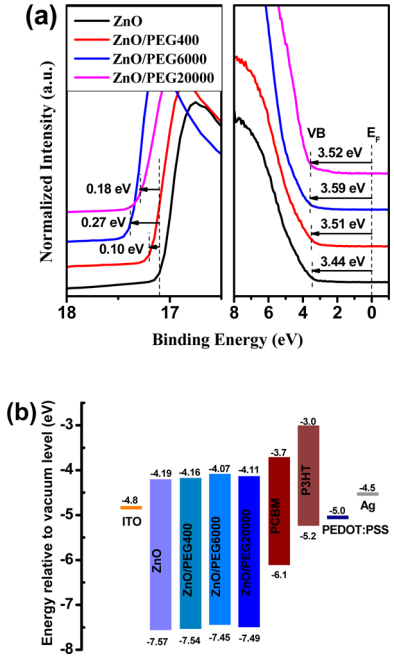

Figure 9. (a) UPS spectra of ZnO, ZnO/PEG400, ZnO/PEG6000, and ZnO/PEG20000 and (b) the corresponding energy level diagram of the components of the device.

estimated LUMO energy levels were −4.19, −4.16, −4.07, and−-4.11 eV for ZnO, ZnO/PEG400, ZnO/PEG6000 and ZnO/PEG20000 film, respectively(Table 4). The optical band gap of ZnO and ZnO/PEG hybrids was estimated using the following equation[44]

$$(\alpha h\nu)^2 = a(h\nu - E_g)$$

where a is a constant and α is the extinction coefficient of ZnO. The effective work function of ZnO/PEG is decreased with respect to pristine ZnO film. The decreased effective work

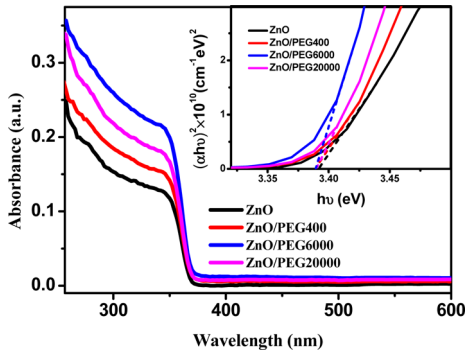

Figure 10. UV−vis absorbance spectra (the inset is plots of $(\alpha h\nu)^2$ versus energy) of ZnO, ZnO/PEG400, ZnO/PEG6000, and ZnO/PEG20000 films.

Table 4. Energy Levels of ZnO, ZnO/PEG400, ZnO/PEG6000, and ZnO/PEG20000

	E_g (UV−vis)	HOMO (UPS)	LUMO (E_g)
ZnO	3.38	7.57	4.19
ZnO/PEG400	3.38	7.54	4.16
ZnO/PEG6000	3.38	7.45	4.07
ZnO/PEG20000	3.38	7.49	4.11

function of ZnO/PEG hybrids cathode buffer layer can lead to large build-in potential and consequently improve charge collection. The decreased effective work function of ZnO/PEG film may be attributed to the fill-up of ZnO surface traps by the lone electron pair of oxygen in PEG backbone, which would restrain the possible trap-assisted interfacial charge recombination.[42] Simultaneously, the conduction band minimum of the ZnO/PEG film is estimated to be located near the LUMO of $PC_{61}BM$. This energy-level alignment facilitates electron injection, consistent with a large forward current and a large photocurrent, which can explain the trend of J_{sc} and the highest value was observed for the devices using ZnO/PEG6000 cathode buffer layer.

To characterize the electron transporting property of the ZnO and ZnO/PEG hybrids cathode buffer layers, we measured the space-charge-limited-current (SCLC) of the cathode buffer layers by using electron-only devices, inset of Figure 11 showed the device architecture. The electron

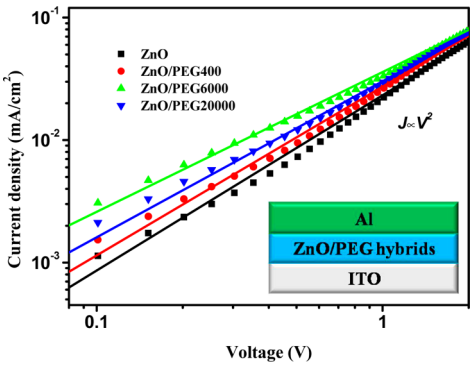

Figure 11. Log J vs log V plots for Mott−Gurney SCLC fitting of the electron-only devices using ZnO, ZnO/PEG400, ZnO/PEG6000, and ZnO/PEG20000 films, and the inset was the architecture of electron-only device.

dx.doi.org/10.1021/am4013038 | ACS Appl. Mater. Interfaces 2013, 5, 5763−5770

mobility was calculated using the Mott–Gurney SCLC equation[45,46]

$$J = (9/8)\mu_e \varepsilon_0 \varepsilon_r (V^2/L^3)$$

where J is the current density, μ_e is the effective charge carrier mobility, which includes the effect of injection efficiency or traps, ε_0 is the permittivity of free-space, ε_r is the relative dielectric constant, V is the applied voltage, and L is the thickness of the cathode buffer layers. The J–V characteristics of electron-only devices were fitted with the SCLC model shown in Figure 11. The effective electron mobility μ_e were summaried in Table 5. The ZnO/PEG6000 hybrids showed the highest electron mobility of 7.92×10^{-4} cm^2 V^{-1} s^{-1}, which corresponded to approximately a two-fold improvement over the device without PEG.

Table 5. Electron Mobility of ZnO, ZnO/PEG400, ZnO/PEG6000 and ZnO/PEG20000

devices	ZnO	ZnO/PEG400	ZnO/PEG6000	ZnO/PEG20000
electron mobility (cm^2 V^{-1} s^{-1})	4.39×10^{-4}	4.96×10^{-4}	7.92×10^{-4}	6.48×10^{-4}

Figure 12 compared the PCE decay of the PSCs with pristine ZnO and ZnO/PEG hybrids cathode buffer layers. The PSCs

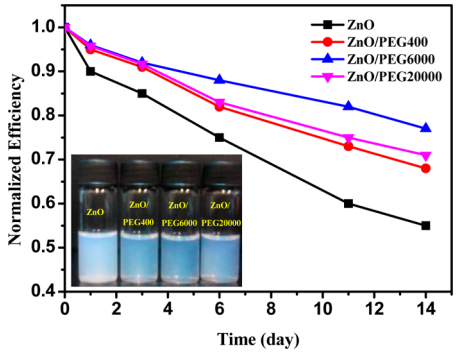

Figure 12. Normalized efficiency decay of PSCs with ZnO, ZnO/PEG400, ZnO/PEG6000 and ZnO/PEG20000 as cathode buffer layers at ambient atmosphere. The inset is the photo of ZnO, ZnO/PEG400, ZnO/PEG6000, and ZnO/PEG2000 solution in a mixture of methanol and 1-butanol (1:1, v/v) for 2 weeks.

were exposed continuously to air at room temperature without any encapsulation barrier. The air stability was significantly increased by introduction of ZnO/PEG hybrids cathode buffer layers, which can be contributed to the stability of the ZnO/PEG hybrids. It can be observed that the ZnO/PEG hybrids kept stable over 2 weeks, whereas the pristine ZnO solution remained slightly translucent and unstable (see the inset of Figure 12). Figure S5 in the Supporting Information showed the TEM images of ZnO, ZnO/PEG400, ZnO/PEG6000, and ZnO/PEG20000 after 2 weeks. We found that the variation of the morphologies of ZnO hybrided with different PEG after 2 weeks had the same trend in the film state with that in the solution state. It was indicated that PEG can effectively suppress ZnO nanoparticles to form large aggregates.

4. CONCLUSIONS

In conclusion, efficient and air-stable flexible inverted polymer solar cells based on P3HT:$PC_{61}BM$ blends were fabricated by using solution-processed ZnO/PEG hybrids as cathode buffer layers. The results showed that the PEG of different molecular weights could effectively passivate the surface traps of ZnO, suppress the interfacial charge recombination, decrease the work function, and improve the energy-level alignment between ZnO and $PC_{61}BM$. Meanwhile, it revealed that the molecular weight of the PEG plays an important role in the performance of flexible inverted polymer solar cells. The shorter PEG backbone (eg. M_w = 400) could not effectively passivate ZnO surface traps with less lone electron pair of oxygen, whereas longer PEG backbone (eg. M_w = 20000) could lead to the formation of the charge transport barrier because of the insulating nature of PEG. As a result, the devices with ZnO/PEG6000 hybrids exhibited the best performance. Due to the simplicity and low-temperature process, it is expected that the use of the ZnO/PEG hybrids as a buffer layer provide the possibility for large area roll-to-roll manufacturing of stable printed polymer solar cells.

■ ASSOCIATED CONTENT

Supporting Information

Text giving the optical transmission spectra; XRD patterns; water contact angle of ZnO, ZnO/PEG400, ZnO/PEG6000, and ZnO/PEG20000; water contact angle of ZnO and ZnO hybridized with different concentrations of PEG6000; and TEM images of ZnO, ZnO/PEG400, ZnO/PEG6000, and ZnO/PEG20000 after 2 weeks. This material is available free of charge via the Internet at http://pubs.acs.org/.

■ AUTHOR INFORMATION

Corresponding Author

*E-mail: ywchen@ncu.edu.cn. Tel.: +86 791 83969562. Fax: +86 791 83969561.

Notes

The authors declare no competing financial interest.

■ ACKNOWLEDGMENTS

The financial support for this work was provided by the National Natural Science Foundation of China (51073076, 51273088, and 51172103).

■ REFERENCES

(1) Yu, G.; Gao, J.; Hummelen, J. C.; Wudl, F.; Heeger, A. J. *Science* **1995**, *270*, 1789–1791.
(2) Po, R.; Carbonera, C.; Bernardi, A.; Camaioni, N. *Energy Environ. Sci.* **2011**, *4*, 285–310.
(3) Krebs, F. C.; Fyenbo, J.; Jorgensen, M. *J. Mater. Chem.* **2010**, *20*, 8994–9001.
(4) Small, C. E.; Chen, S.; Subbiah, J.; Amb, C. M.; Tsang, S.-W.; Lai, T.-H.; Reynolds, J. R.; So, F. *Nat. Photon.* **2012**, *6*, 115–120.
(5) Liang, Y.; Yu, L. *Acc. Chem. Res.* **2010**, *43*, 1227–1236.
(6) Park, S. H.; Roy, A.; Beaupre, S.; Cho, S.; Coates, N.; Moon, J. S.; Moses, D.; Leclerc, M.; Lee, K.; Heeger, A. J. *Nat. Photon.* **2009**, *3*, 297–302.
(7) Blouin, N.; Michaud, A.; Gendron, D.; Wakim, S.; Blair, E.; Neagu-Plesu, R.; Belletete, M.; Durocher, G.; Tao, Y.; Leclerc, M. *J. Am. Chem. Soc.* **2008**, *130*, 732–742.
(8) Ma, W.; Yang, C.; Gong, X.; Lee, K.; Heeger, A. J. *Adv. Funct. Mater.* **2005**, *15*, 1617–1622.
(9) Li, G.; Shrotriya, V.; Huang, J.; Yao, Y.; Moriarty, T.; Emery, K.; Yang, Y. *Nat. Mater.* **2005**, *4*, 864–868.

(10) Lungenschmied, C.; Dennler, G.; Neugebauer, H.; Sariciftci, S. N.; Glatthaar, M.; Meyer, T.; Meyer, A. *Sol. Energy Mater. Sol. Cells* **2007**, *91*, 379−384.
(11) Brabec, C. J.; Gowrisanker, S.; Halls, J. J. M.; Laird, D.; Jia, S.; Williams, S. P. *Adv. Mater.* **2010**, *22*, 3839−3856.
(12) de Jong, M. P.; van Ijzendoorn, L. J.; de Voigt, M. J. A. *Appl. Phys. Lett.* **2000**, *77*, 2255−2257.
(13) Wong, K. W.; Yip, H. L.; Luo, Y.; Wong, K. Y.; Lau, W. M.; Low, K. H.; Chow, H. F.; Gao, Z. Q.; Yeung, W. L.; Chang, C. C. *Appl. Phys. Lett.* **2002**, *80*, 2788−2790.
(14) Sun, Y.; Seo, J. H.; Takacs, C. J.; Seifter, J.; Heeger, A. J. *Adv. Mater.* **2011**, *23*, 1679−1683.
(15) Liang, Z.; Zhang, Q.; Wiranwetchayan, O.; Xi, J.; Yang, Z.; Park, K.; Li, C.; Cao, G. *Adv. Funct. Mater.* **2012**, *22*, 2194−2201.
(16) Huang, J.; Yin, Z. G.; Zheng, Q. D. *Energy Environ. Sci.* **2011**, *4*, 3861−3877.
(17) Roest, A. L.; Kelly, J. J.; Vanmaekelbergh, D.; Meulenkamp, E. A. *Phys. Rev. Lett.* **2002**, *89*, 036801.
(18) Sun, B.; Sirringhaus, H. *Nano Lett.* **2005**, *5*, 2408−2413.
(19) Jo, S. B.; Lee, J. H.; Sim, M.; Kim, M.; Park, J. H.; Choi, Y. S.; Kim, Y.; Ihn, S. G.; Cho, K. *Adv. Energy. Mater.* **2011**, *1*, 690−698.
(20) Yip, H.-L.; Hau, S. K.; Baek, N. S.; Ma, H.; Jen, A. K. Y. *Adv. Mater.* **2008**, *20*, 2376−2382.
(21) Bulliard, X.; Ihn, S.-G.; Yun, S.; Kim, Y.; Choi, D.; Choi, J.-Y.; Kim, M.; Sim, M.; Park, J.-H.; Choi, W.; Cho, K. *Adv. Funct. Mater.* **2010**, *20*, 4381−4387.
(22) Seo, H. O.; Park, S.-Y.; Shim, W. H.; Kim, K.-D.; Lee, K. H.; Jo, M. Y.; Kim, J. H.; Lee, E.; Kim, D.-W.; Kim, Y. D.; Lim, D. C. *J. Phys. Chem. C* **2011**, *115*, 21517−21520.
(23) Ha, Y. E.; Jo, M. Y.; Park, J.; Kang, Y.-C.; Yoo, S. I.; Kim, J. H. *J. Phys. Chem. C* **2013**, *117*, 2646−2652.
(24) Shao, S.; Zheng, K.; Pullerits, T.; Zhang, F. *ACS Appl. Mater. Interfaces* **2013**, *5*, 380−385.
(25) Park, B.; Lee, J.-H.; Chang, M.; Reichmanis, E. *J. Phys. Chem. C* **2012**, *116*, 4252−4258.
(26) Beek, W. J.; Wienk, M. M.; Kemerink, M.; Yang, X.; Janssen, R. A. *J. Phys. Chem. B* **2005**, *109*, 9505−9516.
(27) Gong, X.; Tong, M.; Brunetti, F. G.; Seo, J.; Sun, Y.; Moses, D.; Wudl, F.; Heeger, A. J. *Adv. Mater.* **2011**, *23*, 2272−2277.
(28) Yang, T. B.; Wang, M.; Duan, C. H.; Hu, X. W.; Huang, L.; Peng, J. B.; Huang, F.; Gong, X. *Energy Environ. Sci.* **2012**, *5*, 8208−8214.
(29) Wang, D. H.; Lee, H. K.; Choi, D.-G.; Park, J. H.; Park, O. O. *Appl. Phys. Lett.* **2009**, *95*, 043505−043507.
(30) Kyaw, A. K. K.; Sun, X. W.; Jiang, C. Y.; Lo, G. Q.; Zhao, D. W.; Kwong, D. L. *Appl. Phys. Lett.* **2008**, *93*, 221107−221109.
(31) Jin, H.; Tao, C.; Velusamy, M.; Aljada, M.; Zhang, Y.; Hambsch, M.; Burn, P. L.; Meredith, P. *Adv. Mater.* **2012**, *24*, 2572−2577.
(32) Zeng, H.; Duan, G.; Li, Y.; Yang, S.; Xu, X.; Cai, W. *Adv. Funct. Mater.* **2010**, *20*, 561−572.
(33) Vanheusden, K.; Seager, C. H.; Warren, W. L.; Tallant, D. R.; Voigt, J. A. *Appl. Phys. Lett.* **1996**, *68*, 403−405.
(34) Zhang, S. B.; Wei, S. H.; Zunger, A. *Phys. Rev. B* **2001**, *63*, 075205−075211.
(35) Studenikin, S. A.; Golego, N.; Cocivera, M. *J. Appl. Phys.* **1998**, *84*, 2287−2294.
(36) Sui, X.; Shao, C.; Liu, Y. *Polymer* **2007**, *48*, 1459−1463.
(37) Lee, H. S.; Kim, D. H.; Cho, J. H.; Hwang, M.; Jang, Y.; Cho, K. *J. Am. Chem. Soc.* **2008**, *130*, 10556−10564.
(38) Horowitz, G.; Hajlaoui, M. E. *Synth. Met.* **2001**, *122*, 185−189.
(39) Natsume, Y.; Sakata, H. *Thin Solid Films* **2000**, *372*, 30−36.
(40) Bong, H.; Lee, W. H.; Lee, D. Y.; Kim, B. J.; Cho, J. H.; Cho, K. *Appl. Phys. Lett.* **2010**, *96*, 192115−192117.
(41) Sirringhaus, H. *Adv. Mater.* **2005**, *17*, 2411−2425.
(42) Jo, S. B.; Lee, J. H.; Sim, M.; Kim, M.; Park, J. H.; Choi, Y. S.; Kim, Y.; Ihn, S.-G.; Cho, K. *Adv. Energy Mater.* **2011**, *1*, 690−698.
(43) Braun, S.; Salaneck, W. R.; Fahlman, M. *Adv. Mater.* **2009**, *21*, 1450−1472.
(44) Woo, K.; Kim, Y.; Moon, J. *Energy Environ. Sci.* **2012**, *5*, 5340−5345.
(45) Park, J. S.; Lee, J. M.; Hwang, S. K.; Lee, S. H.; Lee, H. J.; Lee, B. R.; Park, H. I.; Kim, J. S.; Yoo, S.; Song, M. H.; Kim, S. O. *J. Mater. Chem.* **2012**, *22*, 12695−12700.
(46) Park, H.-Y.; Lim, D.; Kim, K.-D.; Jang, S.-Y. *J. Mater. Chem. A* **2013**, *1*, 6327−6334.